Acta Oceanol. Sin., 2024, Vol. 43, No. 9, P. 70–80
https://doi.org/10.1007/s13131-024-2350-7
http://www.aosocean.com
E-mail: ocean2@hyxb.org.cn

Influence of typhoon MITAG on the Kuroshio intrusion in the Luzon Strait during early fall 2019

Meng Liu[1], Fukang Qi[1, 2], Yunpeng Lin[1], Yuping Yang[1], Jingping Xu[1]*

[1] Department of Ocean Science and Engineering, Southern University of Science and Technology, Shenzhen 518055, China

[2] College of Marine Geosciences, Ocean University of China, Qingdao 266100, China

Received 31 October 2023; accepted 27 December 2023

Abstract

Typhoons in the western Pacific have a significant impact on the transport of heat, salt and particles through the Luzon Strait. However, there are very limited field observations of this impact because of extreme difficulties and even dangers for ship-based measurements during the rough weather. Here, we present the preliminary results from analyzing a dataset collected by a glider deployed west of the Luzon Strait a few days prior to the arrival of typhoon MITAG. The gilder data revealed an abnormally salinity (>34.8) subsurface water apparently sourced from Kuroshio intrusion during the typhoon. When typhoon MITAG traveled on the east of the Luzon Strait, the positive wind stress curl strengthened the cyclonic eddy and weakened the anti-cyclonic eddy. This led to a slowdown of Kuroshio and made its intrusion easier. The main axis of the Kuroshio at the northern part of the strait shifted westward after the typhoon and did not return to its original position until a week later. The Ekman transport from persistent northerly wind of typhoon MITAG was significant, but its importance in enhancing the Kuroshio intrusion is only secondary relative to the eddies variations.

Key words: typhoon, glider, Kuroshio intrusion, Luzon Strait

Citation: Liu Meng, Qi Fukang, Lin Yunpeng, Yang Yuping, Xu Jingping. 2024. Influence of typhoon MITAG on the Kuroshio intrusion in the Luzon Strait during early fall 2019. Acta Oceanologica Sinica, 43(9): 70–80, doi: 10.1007/s13131-024-2350-7

1 Introduction

The South China Sea (SCS) is a semi-closed deep-water basin, with the Luzon Strait severing as the primary channel for the water exchange between the northwestern Pacific Ocean and the SCS (Qu, 2002; Tian et al., 2006). The Kuroshio, originating from the North Equator Current, flows northward along the Philippine coast. As it passes though the east side of the Luzon Strait, some of the high-temperature and high-salinity waters of Kuroshio intrude into the SCS (Caruso et al., 2006; Liang et al., 2008), influencing its thermohaline characteristics and playing a vital role in regulating the dynamic and ecological environment of the northeast SCS (Guo et al., 2017; Liu et al., 2020). The mode and path of Kuroshio intrusion, as well as the Luzon Strait transport, show notable seasonality under the influence of the East Asian monsoon (Qu, 2000; Centurioni et al., 2004; Nan et al., 2015; Zhang et al., 2015; Qian et al., 2018). The westward transport across the Luzon Strait is stronger in winter and followed by spring, with a minimum occurring mainly in summer. Ekman transport caused by the northeasterly winter monsoon enhances the westward Luzon Strait transport (Wu and Hsin, 2012). Meanwhile, mesoscale eddies, especially anti-cyclonic eddies shedding from the loop current, significantly contribute to transport in the Luzon Strait (Lien et al., 2014; Yang et al., 2019; Wang et al., 2021).

In addition, intense synoptic-scale events like frequent tropical cyclones (typhoons) in summer and autumn can significantly disrupt the flow in the Luzon Strait. For instance, Chang et al. (2010) revealed that typhoons could directly alter the surface flows of the Kuroshio, persisting for over two days as evidenced by deployed drifters. Chen et al. (2010) used two ADCP mooring systems to examine the response of upper ocean to typhoons, discovering that they modulated the surface current of the Kuroshio and increased anomalous surface water transport exchange across the Luzon Strait due to strong Ekman divergence. Based on *in-situ* measurements, Liu et al. (2020) observed Kuroshio intrusion after typhoon Linfa, which lasted for two weeks and inhibited the increase of Chlorophyll *a* concentration in the northeast SCS.

Due to the challenge of obtaining field observations, many researchers have employed numerical model and satellite data to study typhoon impacts on Luzon Strait transport. Using the POM model, Hsin et al. (2010) revealed that local typhoon-induced wind caused southward-velocity events in the Kuroshio current in the Luzon Strait, also strengthened the Kuroshio intrusion. Hsu et al. (2018), based on simulation results, found that Kuroshio currents would increase (decrease) to the right (left) of the moving typhoon track due to its counterclockwise rotation. By analyzing the results from HYCOM, Sui et al. (2018), analyzing HYCOM results, identified that the typhoon Dandelion passing across the Luzon Strait induced strong westward zonal current at a 50 m depth, primarily related to Ekman transport. Gao et al. (2022) used the COAWST model to analyze the impact of the typhoon Hongxia passing east of the Luzon Strait on the Kuroshio path and intrusion. They determined that the most significant Kuroshio intrusion occurred at 21°N and was strongest in the

Foundation item: The fund from Science, Technology and Innovation Commission of Shenzhen Municipality under contract No. JCYJ20210324105211031; the National Natural Science Foundation of China under contract No. 41720104001.
*Corresponding author, E-mail: xujp@sustech.edu.cn

subsurface layer, with the maximum intrusion flux doubling during the typhoon. These studies show that typhoons could directly change the flow field in the upper ocean, affect the flow state of the Kuroshio, and cause strong anomalies in the Luzon Strait, which can last for several days or even weeks.

Moreover, some studies suggested that tropical cyclones affected the Kuroshio main axis by modulating mesoscale eddies in the upper ocean. Sun et al. (2009) found that typhoons could enhance existing cyclonic eddies through upwelling, subsequently altering the Kuroshio main axis near Japan, and they also pointed out that not all passing typhoons would change the surface eddies. Based on satellite altimeter data, Liu and Hu (2012) noted that the Kuroshio main axis would bend westward when an anticyclonic eddy moved toward the Luzon Strait, facilitating Kuroshio intrusion, but the velocity change of Kuroshio main axis and the process of Kuroshio intrusion caused by typhoons were not described. Moreover, due to the small offset range of the Kuroshio main axis, the validation of the Kuroshio intrusion was lacking of measured data. And beyond that, anti-cyclonic or cyclonic eddies at the typhoon center or edge response differently to passing typhoons (Zhou et al., 2017; He et al., 2024), leading to varying impacts on the Kuroshio main axis. Because of the variable mesoscale eddies near the Kuroshio current in the Luzon Strait, typhoons with different trajectories and intensities have different effects on them, resulting in different degrees of the Kuroshio intrusion. Nevertheless, there are limited reports on Kuroshio changes induced by mesoscale eddy variations in the Luzon Strait under the influence of tropical cyclones, especially the lack of synchronized measurement data to verify the Kuroshio intrusion.

In this study, we used an underwater glider for autonomous and frequent observation in the Luzon Strait during typhoon MITAG. The glider provided continuous vertical profiles of temperature and salinity (Ma et al., 2018; Li et al., 2020). We analysized the data collected over a 13-d measurement period from one glider, and combined with Argo and satellite data to examine the impact of typhoon on eddies and Kuroshio intrusion, as well as to explore the underlying mechanisms. Section 2 details the dataset and methods used. Section 3 outlines the observations made using the glider, while Section 4 delves into the analysis of the related physical processes. Finally, Section 5 offers the conclusions of the study.

2 Data and methods

2.1 *Study area*

The Luzon Strait is located between the Taiwan Island and Luzon Island, spanning from 18.5°N to 22°N, covering a distance of over 350 km, with a maximum depth exceeding 3 000 m. It serves as the only channel for material exchange between the northwestern Pacific Ocean and the SCS. The study area is situated in the East Asian monsoon region. During summer, the southwest monsoon dominates with weak winds, which is not favorable for Kuroshio intrusion. In contrast, the northeast monsoon prevails during winter, bringing strong winds that facilitates Kuroshio intrusion (Yuan et al., 2006). In addition, the study area is affected by tropical cyclones from the northwestern Pacific Ocean, which frequently occur from July to October. When tropical cyclones form, they have the potential to move northwest or turn northward near the Luzon Stait, affecting nearby waters (Sun et al., 2017).

2.2 *Typhoon MITAG*

Typhoon No. 1918 MITAG originated as a tropical depression in the Northwest Pacific (13°N, 138.9°E) at 08:00 (UTC+8) on September 27, 2019. It passed east of the Luzon Strait and Taiwan Island as a typhoon with a maximum wind speed of 40 m/s and a translation speed range of 20–40 km/h from 05:00 on September 29 to 00:00 on October 1 (Fig. 1). Typhoon data were obtained from the Typhoon Network of the Central Meteorological Observatory (NMCS, http://typhoon.nmc.cn). The study area was primarily influenced by the southeast monsoon, and the degree

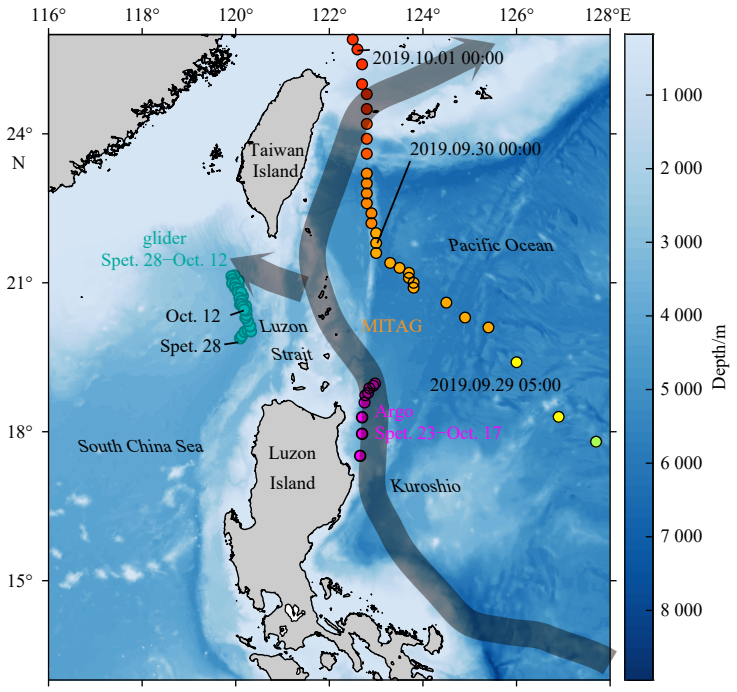

Fig. 1. Typhoon MITAG tracks, glider paths (cyan dots), and the locations of Argo floats (magenta dots). The black shadow indicates the Kuroshio.

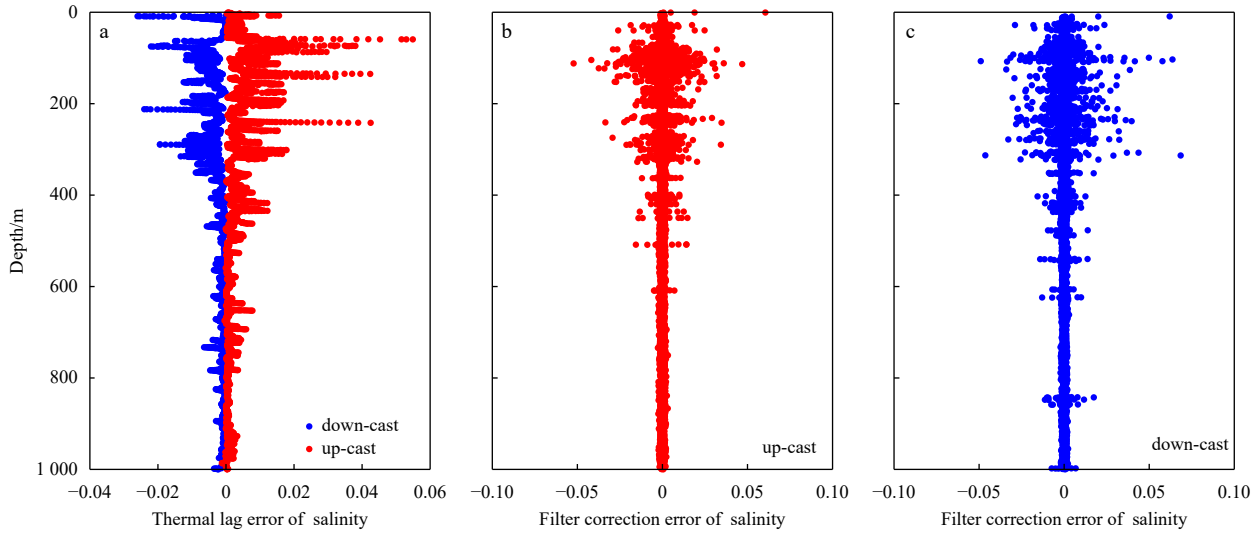

Fig. 2. Corrected errors (Profile 19) including thermal lag correction and burring of salinity.

of Kuroshio intrusion was weak before the observation period.

2.3 *Glider data*

Gliders are a data collecting vehicle that is capable of diving and ascending, by adjusting its in-water buoyancy, along an underwater saw-tooth trajectory, or maintaining gliding mode using hydrodynamic force (Wang et al., 2017). The Petrel-4000 glider (Wang et al., 2017) used in this study equipped with an Idronaut OS304 Plus CTD that records depths from 0 m to 7 000 m with accuracy of 0.05% F.S. (full scale) and resolution of 0.001 5% F.S.; temperatures from –5℃ to 35℃ with accuracy of 0.002 and resolution of 0.000 1; and conductivities from 0 mS/cm to 90 mS/cm with accuracy of 0.003 and resolution of 0.000 3 (Idronaut, 2019). This type of glider has been used in several field studies with satisfactory reliability (Ma et al., 2018; Li et al., 2019, 2020). One Petrel-4000 glider was deployed on 14 September 2019 in northeastern SCS (Fig. 1). Its primary goal was to measure temperature and salinity profiles along the upper reach of the Manila Trench coordinated by a different research project (Liu et al., 2023). In 41 d until recovery on October 25, 2019, a total of 35 valid temperature and salinity profiles (from September 28 to October 12), sampled at 1 Hz, were recorded (Figs 1a and b). For this study, only the data in depth range of 0–500 m are used.

The following steps were followed to process data. (1) Thermal lag errors in the conductivity data from unpumped CTD sensors on the glider were corrected using the method proposed by Morison et al. (1994) and Garau et al. (2011). The temperature reported by the CTD showed a slight time-lag behind the actual value inside the conductivity cell, resulting in an error of –0.1 to 0.2, mostly less than ± 0.05 (Fig. 2a). (2) The difference between the salinity before and after being burred by moving average filtering (Liu et al., 2015; Yi et al., 2019) was mostly within ±0.05 (Figs 2b and c), which is of the same order of magnitude as the thermal lag error. (3) The corrected data were interpolated to create a profile with a vertical bin size of 0.5 m (Troupin et al., 2015). For each pair of dives, the measurements of diving and climbing profiles were averaged to produce the binned vertical profile. This profile was assigned to the middle position between the end coordinates of the first dive and the start coordinates of the next dive. The mixed layer depth (MLD) is defined as the depth at which the potential density increase relative to the surface (10 m) equals the increase in surface potential density when the surface temperature decreases by 0.5℃ (de Boyer Montégut et al., 2004; Wang et al., 2023).

2.4 *Auxiliary data*

Monthly climatological temperature and salinity data from World Ocean Atlas 2018 (WOA18), produced by NOAA National Oceanographic Data Center, were obtained from https://www.nodc.noaa.gov/OC5/woa18/ with a horizontal resolution of 0.25°. The data of Argo Float (Serial No. 2902753), released on 29 March 2019, are obtained from ftp://ftp.argo.org.cn/pub/ARGO/global/core/ and included pressure, temperature and salinity measurements. Daily sea level anomaly (SLA) and surface geostrophic current with a horizontal resolution of 0.25° were provided by CMEMS (Copernicus Marine Service, http://marine.copernicus.eu). The wind filed data were obtained from the NCEP Climate Forecast System Version 2 (CFSv2) Selected Hourly Time-Series Products (https://rda.ucar.edu/datasets/ds094.1/), with a spatial resolution of 0.2°.

3 Results

Figure 3 displays data collected by the glider in the depth range of 0–500 m, showing potential temperature, salinity, density, MLD and buoyancy frequency. Notably, the MLD generally correlated with the depth of buoyancy frequency peaks (Fig. 2d), except for a deviation around October 6, likely attributed to advection with northern surface waters. During the passage of typhoon MITAG over the eastern side of the Luzon Strait from September 29 to October 1 (Fig. 1), marked by black and white dashed lines in Fig. 3, the glider was moving northward. Surface (<50 m) temperature exceeded 28.5℃, salinity ranged from 33.4 to 34.2, and the MLD was approximately 20 m. In the subsurface (50 m to 200 m), salinity gradually increased from around 34.60 to 34.78. Following the typhoon, from October 2 to October 6, the glider continued northward. Surface temperatures decreased by 0.5℃ to 1℃, salinity increased by approximately 1, and the MLD deepened to about 40 m. Surface contours of temperature, salinity and density became convex, indicating the presence of an upwelling structure. In the subsurface, there was a high salinity water mass (HSW) with salinity exceeding 34.80 at depths of 80–160 m, with some points reaching above 34.85. The glider went northward to about 21°N and then turned south from October 6.

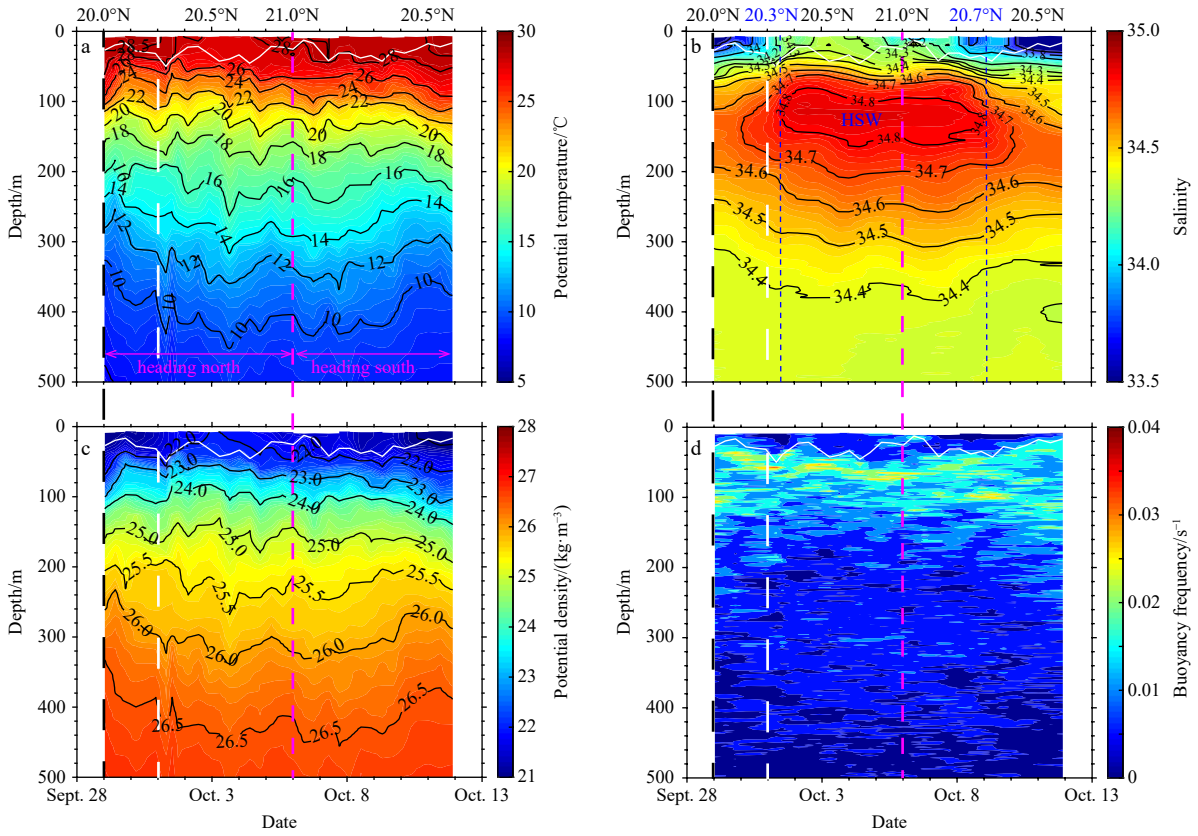

Fig. 3. The time series vertical distribution of potential temperature (a), salinity (b), potential density (c), and calculated buoyancy frequency (d). The latitudes at which the gilder was located on certain days were also marked on the top. The white solid lines denote the MLD, the magenta dashed line indicate that the change in direction of glider, the white and black dashed lines indicate the period of passing east of Luzon Strait for typhoon MITAG (Fig. 1), and the blue dashed lines in b suggest the boundaries of the high salinity water mass (>34.8).

During this southward movement, surface temperatures gradually rose to above 28.5℃, salinity decreased to about 33, and the MLD gradually shallowed to nearly 20 m. Subsurface salinity also gradually decreased to around 34.6. Notably, HSW was observed at 20.3°N on October 1 when glider was moving northward, it was no longer observed at 20.7°N on October 9 during its southward journey. This suggests that the range of HSW in the subsurface had changed approximately nine days after the typhoon.

In order to better distinguish the changes of sea properties during the observation, the time-averaged values of temperature, salinity and density were subtracted from the observed values to acquire their anomaly (Fig. 4). It was clearly seen that after the typhoon (October 1 to 6), the surface and subsurface temperature decreased quickly, while the temperature in the depth of 200 m to 400 m increased slightly (Fig. 4a). When the glider moved northward, the surface and subsurface temperature rebounded somewhat, and the temperature in the depth of 200 m to 400 m changed a little. Due to the presence of HSW, the salinity increased in varying degrees at the depth of 0 m to 400 m from October 1 to 6 (Fig. 4b). Surface and subsurface water were getting colder and saltier, resulting in an increase in density from October 1 to 6, compared to from October 6 to 10 (Fig. 4c). The density in the depth of 200 m to 400 m decreased slightly due to the rise in temperature. The vertical temperature distribution also changed significantly during the observation. Figure 4d is the mean vertical profiles of temperature during September 28 to October 1 (black line), October 1 to 6 (red line), and October 6 to 10 (blue line), respectively. It also shows that the typhoon decreased the surface and subsurface temperature before October 6, and the temperature in the depth of 200 m to 400 m after the typhoon (October 1 to 6, October 6 to 10) was higher than that during the typhoon (September 28 to October 1). It suggested that there were more than one process affecting the seawater properties.

The temperature-salinity (*T*-*S*) diagram was used to determine water characteristics during the observation period (Fig. 5a). Regional average *T*-*S* profiles from WOA18 within the blue and red boxes in the Fig. 5b represent the typical profiles from SCS Water (SCSW) and Kuroshio Water (KW), respectively. It shows that the few upper waters (>25 kg/m^3) from observation stations in the south were similar to the SCSW, while most waters to the north resembled KW, implying that our observations were apparently affected by Kuroshio intrusion.

4 Discussion

4.1 *Variation of the Kuroshio observed by Argo float during the study period*

To the east of the Luzon Strait, an Argo float (Serial No.: 2902753) was deployed on March 29, 2019, and passed by the east of Luzon Island in September and October 2019. The trajectory of float from September 23 to October 17 is shown in Fig. 1 with a 3-d interval. These trajectories located at the path of the Kuroshio (Fig. 1), and the observed temperature and salinity were similar to the KW in the upper layer (Fig. 5a). Also, a recent observation from Ma et al. (2022) found that the core of the Kur-

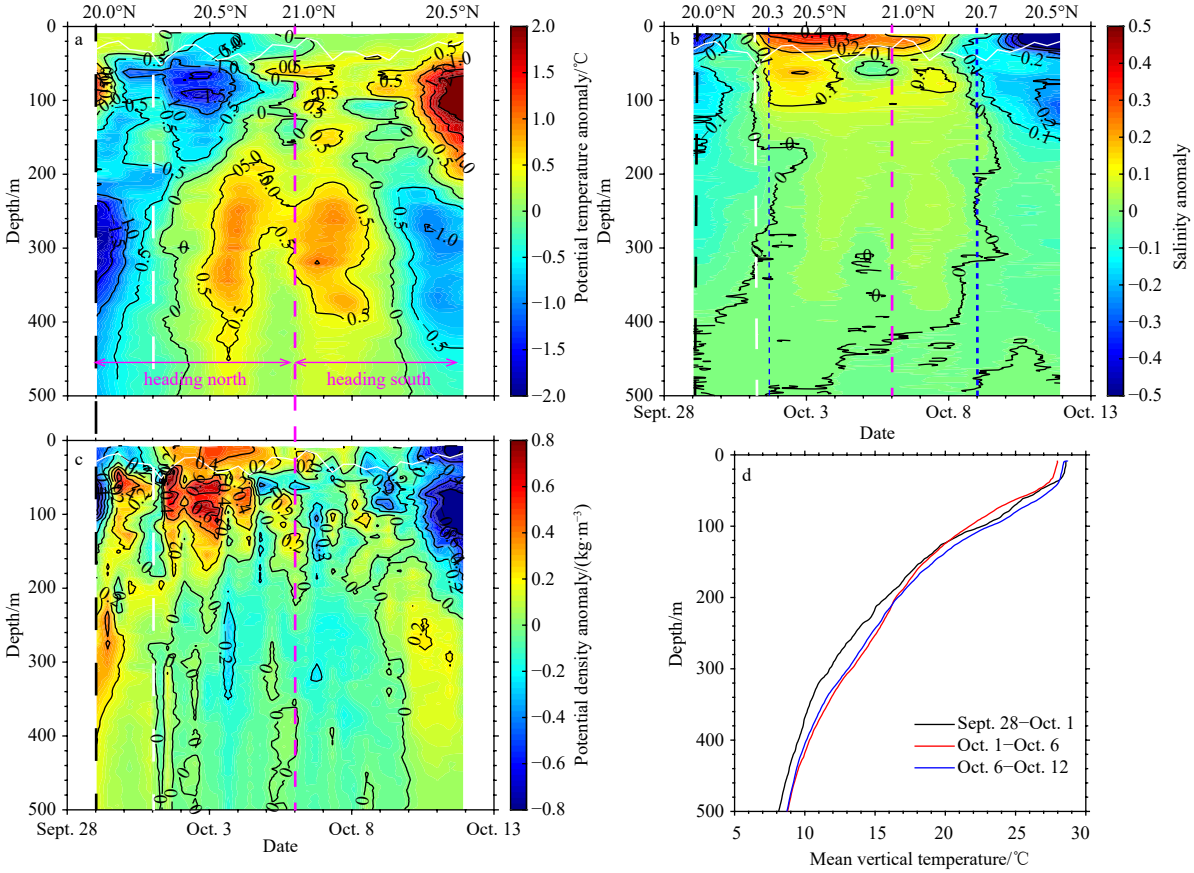

Fig. 4. The time series vertical distribution of potential temperature anomaly (a), salinity anomaly (b), potential density anomaly (c), and mean vertical temperature (d). The latitudes at which the gilder was located on certain days were also marked on the top. The white solid lines denote the MLD, the magenta dashed line indicate that the change in direction of glider, the white and black dashed lines indicate the period of passing east of Luzon Strait for typhoon MITAG (Fig. 1), and the blue dashed lines in b suggest the boundaries of the high salinity water mass (>34.8).

oshio east of Luzon Island was located at 122.7°E, which near the trajectories of the Argo float. Therefore, the Argo dataset could represent the variation in KW during the study period. It revealed that the HSW was mainly distributed at depths ranging from 80–250 m (Fig. 6b), which was deeper than the observations by glider. The subsurface maximum salinity exceeds 38.95. After the typhoon, the surface temperature and salinity decreased by about 0.8℃ and 0.4, respectively (Figs 6a and b). The MLD decreased from around 60 m to 40 m, and the HSW in subsurface was uplifted (Fig. 6b). Until October 9, the surface temperature, salinity and MLD recovered as before.

4.2 *Influence mechanism of Typhoon MITAG on Kuroshio intrusion*

Previous studies have demonstrated that the 34.7 salinity isohaline effectively distinguishes between KW and SCSW (Qu, 2000; Nan et al., 2011; Wang et al., 2021). Kuroshio intrusion inevitably pushes high salinity KW through Luzon Strait and sometimes wells into the SCS (Xue et al., 2004; Caruso et al., 2006). The monthly climatology salinity distributions from WOA18 indicate that KW is widespread west of the Luzon Strait on September and October, but no water with salinity greater than 34.8 has crossed the Luzon Strait (Figs 5b and c). The high salinity (>34.9) in the subsurface from the Argo dataset agreed with the climatology data (Fig. 6b). However, the glider monitoring results indicated an unusually large range of HSW in this season, extending to 20.3°N (Fig. 3b), which is broader when compared to previous observations in same season (Zhou et al., 2009; Huang and Hu, 2010; Wang et al., 2021, 2023).

To explore the processes of HSW intrusion, we plotted the time evolution of sea level anomaly (SLA) and geostrophic currents from September 28 to October 14, 2019 with a 2-d interval (Fig. 7). According to the types of Kuroshio intrusion identified by Nan et al. (2011), the Kuroshio leaped the Luzon Strait before typhoon MITAG. The eastern side of the trajectories of glider corresponded to the Kuroshio main axis, while the western side was the center of a cyclonic eddy. The convex-upward isopycnal in the cyclonic eddy resulted in a decrease in surface temperature, consistent with observations by glider (Figs 3a, b, and c). Meanwhile, the surface water with high temperature (>28.5℃) and low salinity (<34) appeared to originate from the anti-cyclonic eddy south of the observation area (Figs 3a, b, and 7a). Following the typhoon, significant changes were observed in the Kuroshio main axis and the eddies east of the Luzon Strait. In Fig 6a, we defined the Kuroshio main axis location as the longitude with the maximum v-component velocities within the green rectangular area (20.125°–21.875°N, 120.125°–121.875°E) (Kuo et al., 2018) and denoted the cyclonic and anti-cyclonic eddies as “CE” and “AE” (Fig. 7a). Figure 8 depicts the variations in the Kuroshio main axis and related eddies (CE, AE) before and after the typhoon. Prior to the typhoon, the Kuroshio main axis near 21°N was positioned around 121.125°E (Fig. 8a), with a northward velocity of about

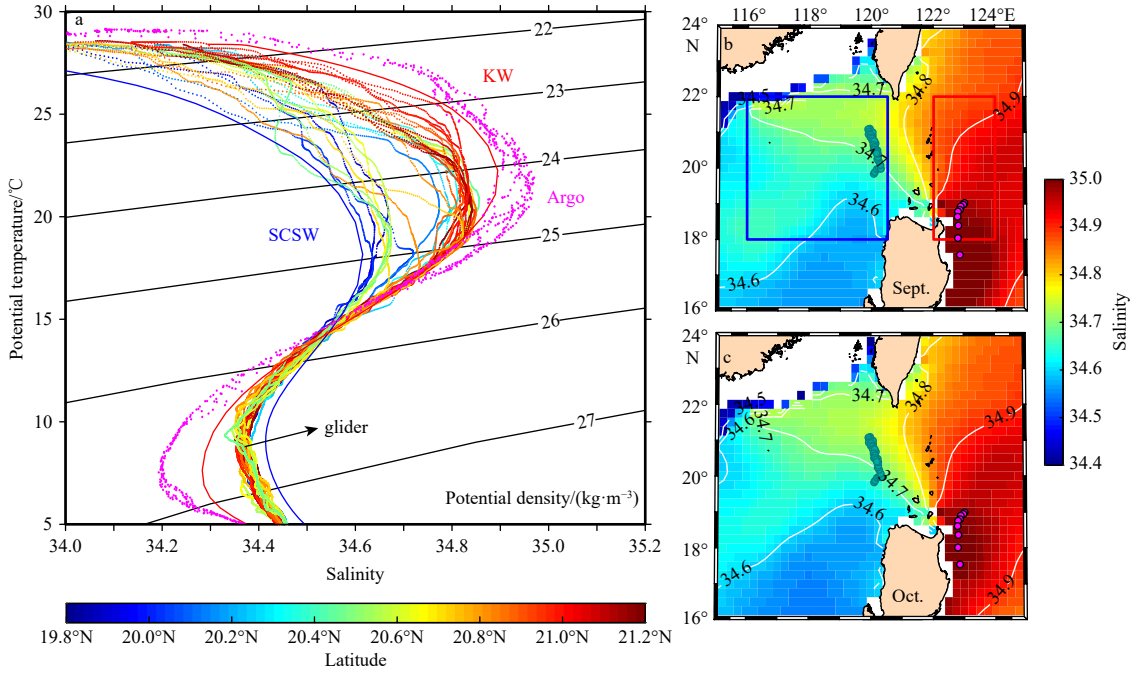

Fig. 5. *T-S* diagrams of CS1/2 and Argo profiles (a) and the climatology salinity maximum at a depth of 0–400 m for September (b) and October (c), respectively. In a, the blue thick line represents the averaged *T-S* curves for the northeastern SCS water (SCSW), the red thick line represents Kuroshio water (KW), based on WOA 18 climatology data, and the black contours represent potential density (σ_θ). The rectangles in b indicate the sampling location of different water masses: the northeastern SCS Water (SCSW, 18°–22°N, 116°–120.5°E) is marked in blue, and the Kuroshio water (KW, 18°–22°N, 122°–124°E) is indicated in red. The cyan dots in c are glider paths, and the magenta dots are locations of Argo floats.

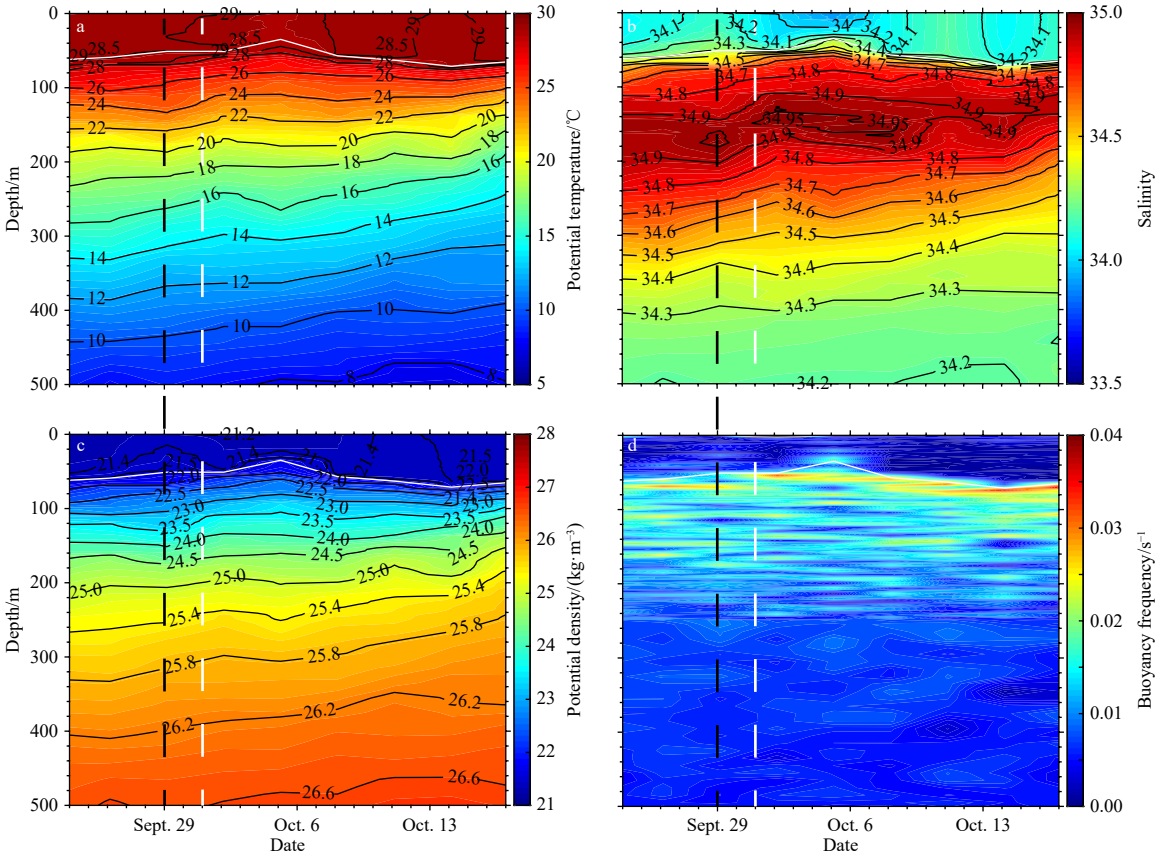

Fig. 6. Potential temperature (a), salinity (b), and potential density (c) by Argo float, respectively, and calculated buoyancy frequency (d). The white solid lines denote the MLD, the white and black dashed lines indicate the period of passing east of Luzon Strait for typhoon MITAG (Fig. 1).

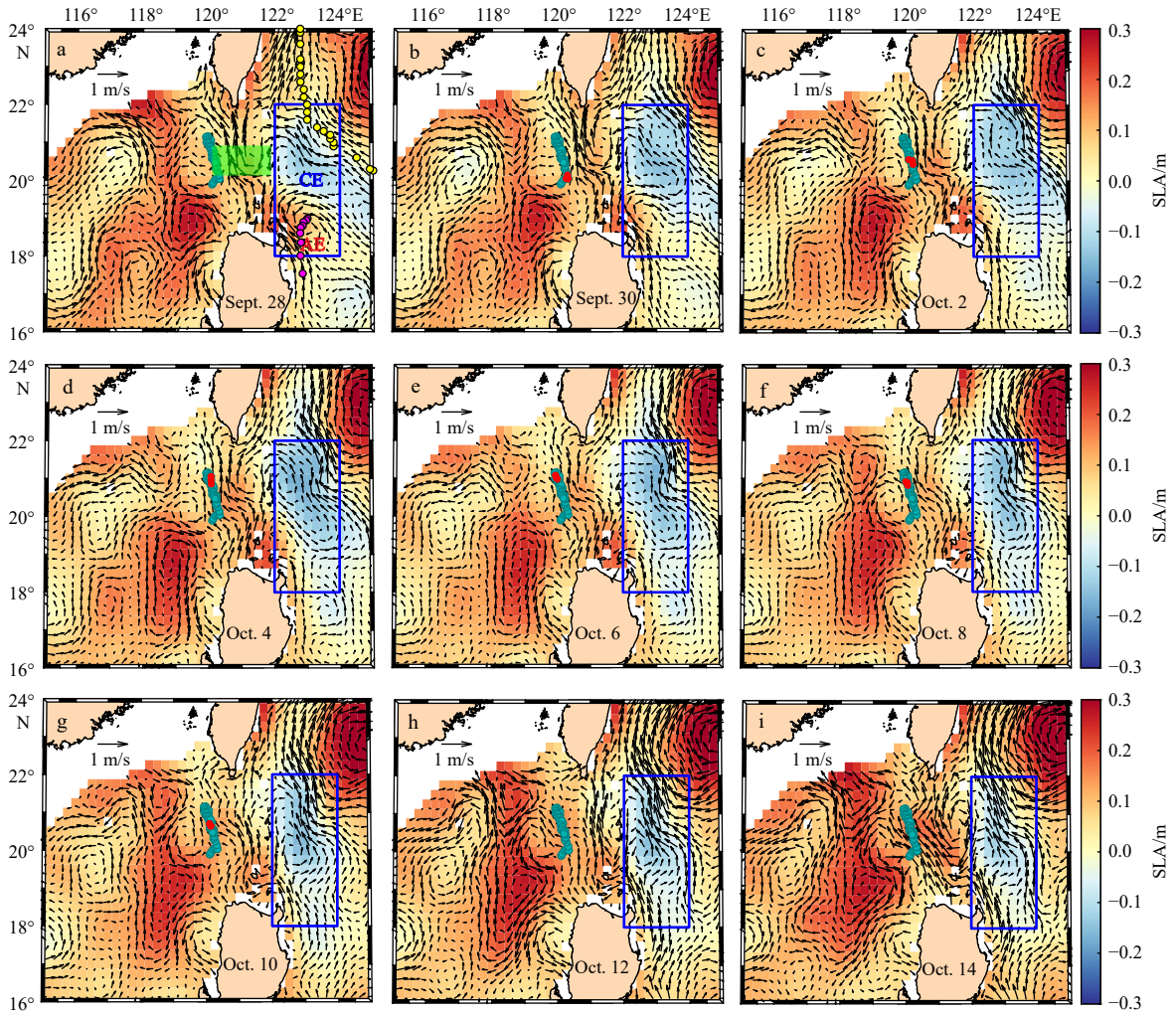

Fig. 7. Time evolution of the SLA (m) and geostrophic currents (m/s) from September 28 to October 14, 2019. Regions shallower than 200 m are masked. The observed section is represented by cyan dots. The positions of the glider during that day are denoted by red dots. The yellow and magenta dots are the trajectories of typhoon and Argo float, respectively. The green rectangular frame is used to show the axis of the Kuroshio current, and the blue boxes is area in which the variations of total relative vorticity and EPV are calculated. The cyclonic and anti-cyclonic eddies in the blue box are denoted as "CE" and "AE".

0.5 m/s (Fig. 8b). During the typhoon, the Kuroshio current weakened by about 0.1 m/s but remained in the same position. After the typhoon, the main axis shifted westward by about 0.5° and its velocity decreased to about 0.25 m/s. It wasn't until October 6 that the main axis returned to its original position, although its velocity did not recover to the initial level (Figs 8a and b). Additionlly, we extracted the velocity magnitude of the Kuroshio upstream (near 18.5°N) during the study period. It exhibited a decrease after the typhoon but rebounded to it initial level after the typhoon on October 6 (Fig. 8c). Therefore, we concluded that the influence of typhoon on the Kuroshio persisted for approximately 7 d, from October 2 to October 9, which aligned with the observations by glider, indicating a deeper MLD (Fig. 3d) and the appearance of HSW (Fig. 3b) during this period eddies in the upper ocean can be influenced by typhoons and may not fully recover in the short term, as noted in previous studies (Sun et al., 2009; Hu et al., 2012; Hsu et al., 2018; Zhang et al., 2023). The variations in SLA and geostrophic currents (Fig. 7), coupled with the increase of total relative vorticity and the decrease of SLA east of the Luzon Strait (blue box in Fig. 7a; Figs 8d and e), suggested that CE was strengthened while AE was weakened after the typhoon. The rise of the pycnocline following the typhoon, as observed from the Argo dataset, might be partially attributed to the weakening of AE (Fig. 6). These changes in the eddies also resulted in a reduction in the velocity of the Kuroshio current. As the Kuroshio flows northward through the Luzon Strait, the β effect and potential vorticity conservation cause it to bend lead clockwise (anti-cyclonic), promoting Kuroshio intrusion. The decrease in Kuroshio velocity renders its main axis more susceptible to this clockwise bending, further facilitating Kuroshio intrusion (Yaremchuk and Qu, 2004; Nan et al., 2015; Gao et al., 2022).

During the course of the typhoon, the turbulent local wind field typically induce vigorous mixing, Ekman pumping and transport, leading to upwelling or downwelling in the upper ocean. Wind curl (S), Ekman pumping velocity (EPV, W_{E}), and Ekman transport were calculated using the equations $S = \frac{\partial v}{\partial x} - \frac{\partial u}{\partial y}$, $W_{\mathrm{E}} = \frac{\nabla \times \tau}{\rho_{\mathrm{s}} f}$ and $M_x = \frac{\tau_y}{f}$, where $\tau = \rho_{\mathrm{a}} C_{\mathrm{D}} u^2$ is the wind stress, $f = 2\omega \sin\theta$ is the Coriolis parameter for latitude θ, ρ_{a}, and ρ_{s} are the densities of air and sea water, respectively, u and v represent wind velocities at 10 m above sea level , ω is the

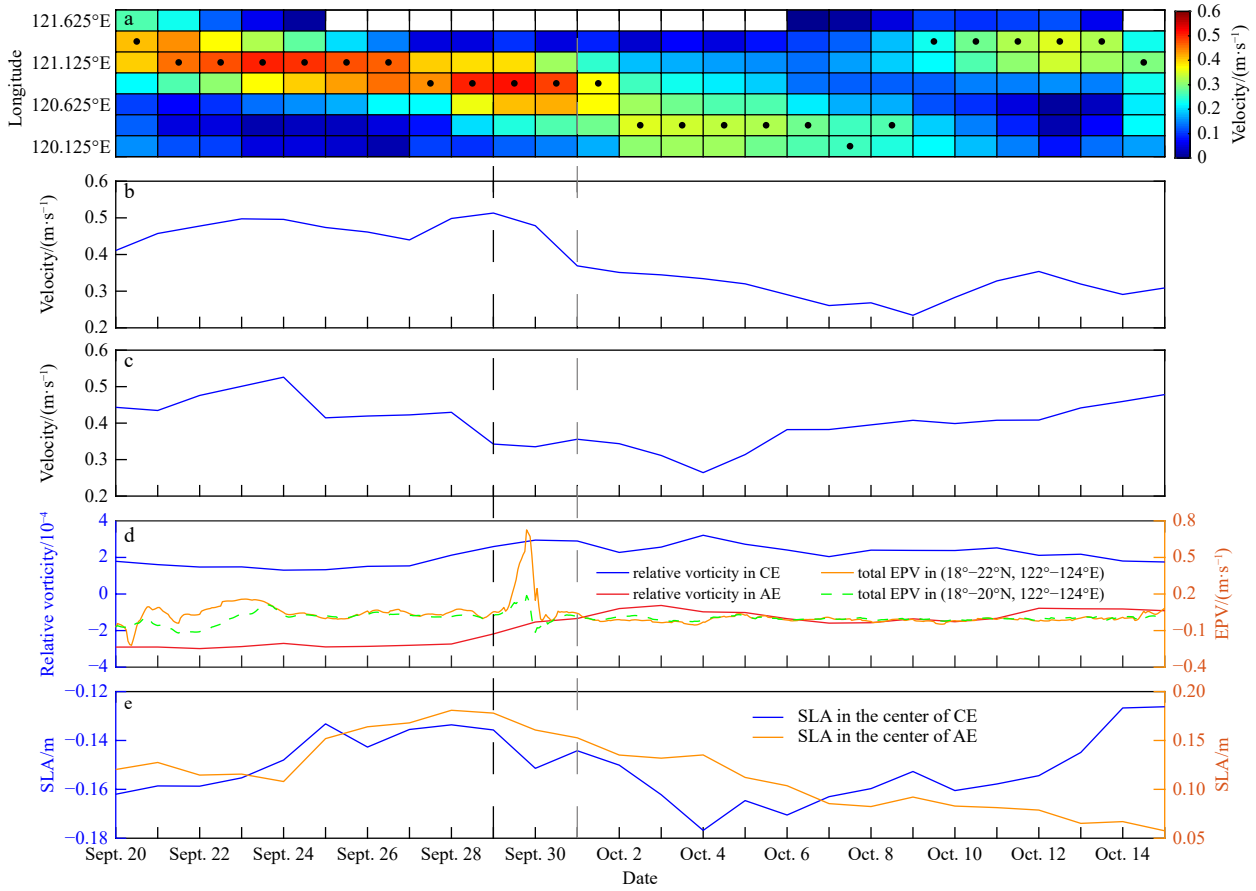

Fig. 8. Variations of the Kuroshio current during the study period, represented by the geostrophic current meridional velocity (m/s). a. The movement of the Kuroshio current axis from 120.125°E to 121.875°E. The contour map indicates the northward meridional vector of the Kuroshio current. Each grid represents a velocity maximum and their longitude in the green rectangular (20.125°–21.875°N, 120.125°–121.875°E) in Fig. 7a. The black dots are the position of the Kuroshio current main axis. b. The velocity variation of the Kuroshio current main axis near 21°N. c. The velocity variation of the Kuroshio current main axis near 18.5°N. d. The variation of total relative vorticity in the CE (blue line) and AE (red line) and EPV (orange and green lines) in the blue box (18°–22°N, 122°–124°E) in Fig. 7. The orange line indicate the total EPV calculated in the box of (18°–22°N, 122°–124°E), and green line indicate the total EPV calculated in the box of (18°–20°N, 122°–124°E). The positive value of EPV indicate the Ekman upwelling. e. The variation of SLA in the center of CE (blue line) and AE (orange line).

rotation rate of the Earth, and C_D is the speed-dependent drag coefficient. Figure 9 illustrates the distribution of wind stress curl and Ekman transport during the typhoon. Positive wind stress curl prevailed to the east of the Luzon Strait (Figs 9a and b), resulting in robust Ekman upwelling (Fig. 8d, orange line) and westward Ekman transport (Figs 9d and e). However, the Kuroshio main axis remained stable, with only a slight velocity decrease (Figs 8a and b), suggesting the typhoon-induced westward Ekman transport was not the direct cause of Kuroshio intrusion. Typhoon MITAG introduced positive potential vorticity to the east of the Luzon Strait (Fig. 8d, blue and red lines), weakening AE and strengthened CE. This led to a significant reduction and westward shift in the Kuroshio main axis, with upper ocean effects lagging by 1–2 d but persisting for nearly 7 d. Generally, the anti-cyclonic eddies at the edges of typhoon intensified due to strong negative wind stress curl (Zhou et al., 2017; He et al., 2024). The wind stress curl at AE alternated between positive and negative EPV (Fig. 8d, green line), with positive curl ultimately dominating and weakening AE. Furthermore, the center of the typhoon was east of the Kuroshio main axis, and northerly winds influenced this axis. This may have caused a buildup of water levels to the Luzon Strait, resulting in a difference in water level with the south and facilitating a geostrophic flow to the west. This, in turn, contributed the westward shift of the Kuroshio main axis (Gao et al., 2022). The frequent occurrence of tropical cyclones (typhoons) near the Luzon Strait likely played a role in the high-frequency disturbances in the Kuroshio intrusion (Hsin et al., 2010). It is worth pointing out, however, that the mechanisms of short-term strengthening of Kuroshio intrusion is likely more complex than the action of eddies. Other factors such as instability of the Kuroshio, Rossby waves responding to remote forcing, among others, may also have contributed to the processes (Lu and Liu, 2013; Nan et al., 2015). More high-resolution observations and numerical modelling efforts are required to untangle these relationships.

The influence of strengthened Kuroshio intrusion was not only in surface and subsurface, but also in the deeper water. The mixing, upwelling and horizontal advection due to passing of typhoon caused the decreased in temperature in the surface and subsurface, but did not affect the deeper regions (>200 m) (Figs 4a and d). The increase in temperature in the depth of 200 m to 400 m was mainly influenced by the Kuroshio water with high temperature and salinity, also the change of salinity also indicated the influence range of Kuroshio intrusion (Fig. 4b).

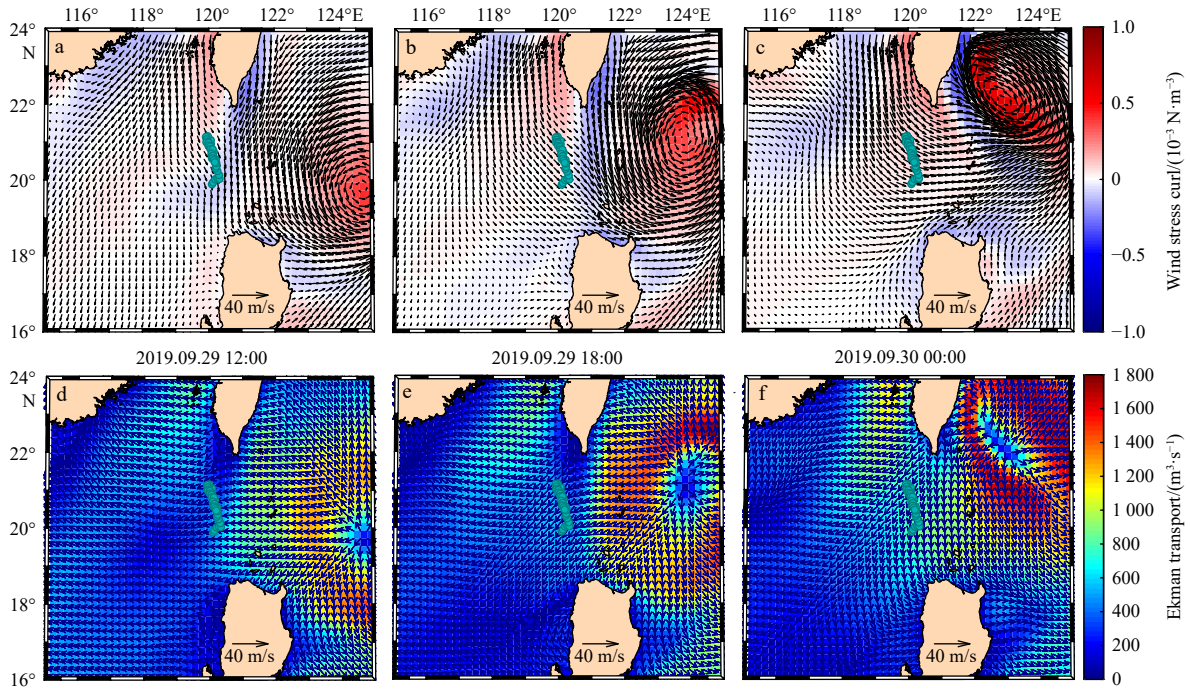

Fig. 9. Distribution of wind field, wind stress curl (a, b, c) and Ekman transport (d, e, f) when the typhoon passed east of the Luzon Strait. The contour maps in a, b, and c display the wind curl, and the arrows indicate the wind velocity and direction. The contour maps in d, e, and f show the Ekman transport per unit width, and the arrows represent directions.

After October 6, the typhoon process weakened and the Kuroshio intrusion increased the surface and subsurface temperature slightly. Finally, the Kuroshio intrusion speeded up the recovering of temperature after the typhoon.

5 Conclusions

In the paper, we used a glider to collect continuous temperature and salinity profiles in the upper ocean west of the Luzon Strait during and after typhoon MITAG. Combining this data with information from Argo floats and satellite, we explored the impact of typhoon on Kuroshio intrusion. After typhoon MATIG, there was a notable intensification of Kuroshio intrusion in the northern Luzon Strait, accompanied by the subsurface entry of the high-salinity water (HSW) into the South China Sea. The Kuroshio main axis shifted westward by up to 0.5°, and its velocity decreased. This enhancement of Kuroshio intrusion lagged the typhoon by 1–2 d but lasted for nearly a week. Importantly, this intensification was not a direct result of Ekman transport, but rather stemmed from changes in the eddies east of the Luzon Strait influenced by typhoon. The typhoon introduced positive wind stress curl into the upper ocean, which weakened the anticyclonic eddy "AE" and strengthened the cyclonic eddy "CE", both located to the right of the Kuroshio main axis. These changes to the eddies resulted in a gradual slow-down and westward shift of the Kuroshio main axis. Nevertheless, more high-resolution observations and numerical modelling efforts are still required to untangle the complex effect of typhoons on Kuroshio's intrusion.

Acknowledgements

We thank Chong Ren, Yanhui Wang, Zhiqiang Liu, Baoduo Wang, Runfeng Zhang, and Chenyi Luo for their help in the provision of instruments, observation conducting, and data processing. We also thank CMEMS (http://marine.copernicus.eu) for the SLA and absolute geostrophic velocity data, the NCEP Climate Forecast System Version 2 (CFSv2) (https://rda.ucar.edu/) for wind field data, Argo float (http://www.argo.ucsd.edu/) for the *in situ* data, and the Typhoon Network of the Central Meteorological Observatory (NMCS, http://typhoon.nmc.cn) for providing typhoon track data.

References

Caruso M J, Gawarkiewicz G G, Beardsley R C. 2006. Interannual variability of the Kuroshio intrusion in the South China Sea. Journal of Oceanography, 62(4): 559–575, doi: 10.1007/s10872-006-0076-0

Centurioni L R, Niiler P P, Lee D K. 2004. Observations of inflow of philippine sea surface water into the South China Sea through the luzon strait. Journal of Physical Oceanography, 34(1): 113–121, doi: 10.1175/1520-0485(2004)034<0113:OOIOPS>2.0.CO;2

Chang Yu-Chia, Tseng Ruo-Shan, Centurioni L R. 2010. Typhoon-induced strong surface flows in the Taiwan Strait and Pacific. Journal of Oceanography, 66(2): 175–182, doi: 10.1007/s10872-010-0015-y

Chen Fei, Du Yan, Yan Li, et al. 2010. Response of upper ocean currents to typhoons at two ADCP moorings west of the Luzon Strait. Chinese Journal of Oceanology and Limnology, 28(5): 1002–1011, doi: 10.1007/s00343-010-0025-z

de Boyer Montégut C, Madec G, Fischer A S, et al. 2004. Mixed layer depth over the global ocean: An examination of profile data and a profile-based climatology. Journal of Geophysical Research: Oceans, 109(C12): C12003

Gao Shumin, Han Shuzong, Wang Shicheng, et al. 2022. The influence of typhoon 'Hongxia' on the intrusion of the Kuroshio current into the South China Sea. Journal of Ocean University of China, 22(2): 297–312

Garau B, Ruiz S, Zhang W G, et al. 2011. Thermal lag correction on slocum CTD glider data. Journal of Atmospheric and Oceanic Technology, 28(9): 1065–1071, doi: 10.1175/JTECH-D-10-05030.1

Guo Lin, Xiu Peng, Chai Fei, et al. 2017. Enhanced chlorophyll concentrations induced by Kuroshio intrusion fronts in the north-

ern South China Sea. Geophysical Research Letters, 44(22): 11565–11572

He Yihao, Lin Xiayan, Han Guoqing, et al. 2024. The different dynamic influences of typhoon kalmaegi on two pre-existing anticyclonic ocean eddies. Ocean Science, 20(2): 621–637, doi: 10.5194/os-20-621-2024

Hsin Yi-Chia, Qu Tangdong, Wu Chau-Ron. 2010. Intra-seasonal variation of the Kuroshio southeast of Taiwan and its possible forcing mechanism. Ocean Dynamics, 60(5): 1293–1306, doi: 10.1007/s10236-010-0294-2

Hsu Taiwen, Chou Meng-Hsien, Chao Weiting, et al. 2018. Typhoon effect on Kuroshio and green island wakes: A modelling study. Atmosphere, 9(2): 36, doi: 10.3390/atmos9020036

Hu Jianyu, Zheng Quanan, Sun Zhenyu, et al. 2012. Penetration of nonlinear Rossby eddies into South China Sea evidenced by cruise data. Journal of Geophysical Research: Oceans, 117(C3): C03010

Huang Zhida, Hu Jianyu. 2010. Hydrographical characteristic along the 20.5°N section through the Luzon Strait based on Argo data. Journal of Oceanography in Taiwan Strait (in Chinese), 29(4): 539–546

Idronaut S R L, 2019. OCEAN SEVEN 304Plus CTD PROBE. Brugherio: Monte Amiata, 9–10

Kuo Yichun, Zheng Zhewen, Zheng Quanan, et al. 2018. Typhoon-Kuroshio interaction in an air-sea coupled system: Case study of typhoon nanmadol (2011). Ocean Modelling, 132: 130–138, doi: 10.1016/j.ocemod.2018.10.007

Li Shufeng, Wang Shuxin, Zhang Fumin, et al. 2019. Constructing the three-dimensional structure of an anticyclonic eddy in the south China sea using multiple underwater gliders. Journal of Atmospheric and Oceanic Technology, 36(12): 2449–2470, doi: 10.1175/JTECH-D-19-0006.1

Li Shufeng, Zhang Fumin, Wang Shuxin, et al. 2020. Constructing the three-dimensional structure of an anticyclonic eddy with the optimal configuration of an underwater glider network. Applied Ocean Research, 95: 101893, doi: 10.1016/j.apor.2019.101893

Liang Wen-Der, Yang Yiing Jang, Tang Tswen Yung, et al. 2008. Kuroshio in the Luzon Strait. Journal of Geophysical Research: Oceans, 113(C8): C08048

Lien R C, Ma B, Cheng Yu-Hsin, et al. 2014. Modulation of Kuroshio transport by mesoscale eddies at the Luzon Strait entrance. Journal of Geophysical Research: Oceans, 119(4): 2129–2142, doi: 10.1002/2013JC009548

Liu Guangping, Hu Jianyu. 2012. A preliminary analysis of variation of the Kuroshio axis during tropical cyclone. Journal of Tropical Oceanography (in Chinese), 31(1): 35–41

Liu Yupeng, Tang Danling, Tang Shilin, et al. 2020. A case study of Chlorophyll a response to tropical cyclone Wind Pump considering Kuroshio invasion and air-sea heat exchange. Science of The Total Environment, 741: 140290, doi: 10.1016/j.scitotenv.2020.140290

Liu Meng, Wang Zhiwen, Yu Kaiqi, et al. 2023. Two distinct types of turbidity currents observed in the Manila Trench, South China Sea. Communications Earth & Environment, 4: 108

Liu Yonggang, Weisberg R H, Lembke C. 2015. Glider salinity correction for unpumped CTD sensors across a sharp thermocline. In: Liu Yonggang, Kerkering H, Weisberg R H, eds. Coastal Ocean Observing Systems. Boston: Academic Press, 305–325.

Lu Jiuyou, Liu Qinyu. 2013. Gap-leaping Kuroshio and blocking westward-propagating Rossby wave and eddy in the Luzon Strait. Journal of Geophysical Research: Oceans, 118(3): 1170–1181, doi: 10.1002/jgrc.20116

Ma Jie, Hu Shijian, Hu Dunxin, et al. 2022. Structure and variability of the Kuroshio and Luzon Undercurrent observed by a mooring array. Journal of Geophysical Research: Oceans, 127(2): e2021JC017754, doi: 10.1029/2021JC017754

Ma Wei, Wang Yanhui, Yang Shaoqiong, et al. 2018. Observation of internal solitary waves using an underwater glider in the northern South China Sea. Journal of Coastal Research, 34(5): 1188–1195

Morison J, Andersen R, Larson N, et al. 1994. The correction for thermal-lag effects in Sea-Bird CTD data. Journal of Atmospheric and Oceanic Technology, 11(4): 1151–1164, doi: 10.1175/1520-0426(1994)011<1151:TCFTLE>2.0.CO;2

Nan Feng, Xue Huijie, Chai Fei, et al. 2011. Identification of different types of Kuroshio intrusion into the South China Sea. Ocean Dynamics, 61(9): 1291–1304, doi: 10.1007/s10236-011-0426-3

Nan Feng, Xue Huijie, Yu Fei. 2015. Kuroshio intrusion into the South China Sea: A review. Progress in Oceanography, 137: 314–333, doi: 10.1016/j.pocean.2014.05.012

Qian Simeng, Wei Hao, Xiao Jingen, et al. 2018. Impacts of the Kuroshio intrusion on the two eddies in the northern South China Sea in late spring 2016. Ocean Dynamics, 68(12): 1695–1709, doi: 10.1007/s10236-018-1224-y

Qu Tangdong. 2000. Upper-layer circulation in the South China Sea. Journal of Physical Oceanography, 30(6): 1450–1460, doi: 10.1175/1520-0485(2000)030<1450:ULCITS>2.0.CO;2

Qu Tangdong. 2002. Evidence for water exchange between the South China Sea and the Pacific Ocean through the Luzon Strait. Acta Oceanologica Sinica, 21(2): 175–185

Sui Junpeng, Chen Haijun, Wang Zhuyu, et al. 2018. Analysis of the Luzon Strait transport anomalies caused by typhoon "Dandelion" in 2004. Marine Forecasts (in Chinese), 35(5): 1–6

Sun Jingru, Oey L, Xu F H, et al. 2017. Sea level rise, surface warming, and the weakened buffering ability of South China Sea to strong typhoons in recent decades. Scientific Reports, 7(1): 7418, doi: 10.1038/s41598-017-07572-3

Sun Liang, Yang Yuanjian, Fu Yunfei. 2009. Impacts of typhoons on the Kuroshio large meander: Observation evidences. Atmospheric and Oceanic Science Letters, 2(1): 45–50, doi: 10.1080/16742834.2009.11446772

Tian Jiwei, Yang Qingxuan, Liang Xinfeng, et al. 2006. Observation of Luzon Strait transport. Geophysical Research Letters, 33(19): L19607

Troupin C, Beltran J P, Heslop E, et al. 2015. A toolbox for glider data processing and management. Methods in Oceanography, 13–14: 13–23

Wang Xiangpeng, Du Yan, Zhang Yuhong, et al. 2021. Influence of two eddy pairs on high-salinity water intrusion in the northern South China Sea during fall-winter 2015/2016. Journal of Geophysical Research: Oceans, 126(6): e2020JC016733, doi: 10.1029/2020JC016733

Wang Xiangpeng, Du Yan, Zhang Yuhong, et al. 2023. Effects of multiple dynamic processes on chlorophyll variation in the Luzon Strait in summer 2019 based on glider observation. Journal of Oceanology and Limnology, 41(2): 469–481, doi: 10.1007/s00343-022-1416-7

Wang Yanhui, Zhang Yiteng, Zhang Mingming, et al. 2017. Design and flight performance of hybrid underwater glider with controllable wings. International Journal of Advanced Robotic Systems, 14(3): 1729881417703566

Wu Chau-Ron, Hsin Y C. 2012. The forcing mechanism leading to the Kuroshio intrusion into the South China Sea. Journal of Geophysical Research: Oceans, 117(C7): C07015

Xue Huijie, Chai Fei, Pettigrew N, et al. 2004. Kuroshio intrusion and the circulation in the South China Sea. Journal of Geophysical Research: Oceans, 109(C2): C02017

Yang Yikai, Wang Dongxiao, Wang Qiang, et al. 2019. Eddy-induced transport of saline Kuroshio water into the northern South China Sea. Journal of Geophysical Research: Oceans, 124(9): 6673–6687, doi: 10.1029/2018JC014847

Yaremchuk M, Qu Tangdong. 2004. Seasonal variability of the large-scale currents near the coast of the Philippines. Journal of Physical Oceanography, 34(4): 844–855, doi: 10.1175/1520-0485(2004)034<0844:SVOTLC>2.0.CO;2

Yi Zhenhui, Yu Jiancheng, Mao Huabin, et al. 2019. A noise processing method for salinity data underwater glider. Journal of Unmanned Undersea Systems (in Chinese), 27(5): 503–513

Yuan Dongliang, Han Weiqing, Hu Dunxin. 2006. Surface Kuroshio path in the Luzon Strait area derived from satellite remote sensing data. Journal of Geophysical Research: Oceans, 111(C11):

C11007

Zhang Zhiwei, Zhao Wei, Tian Jiwei, et al. 2015. Spatial structure and temporal variability of the zonal flow in the Luzon Strait. Journal of Geophysical Research: Oceans, 120(2): 759–776, doi: 10.1002/2014JC010308

Zhang Zheliang, Zheng Yunxia, Li Hao. 2023. Imprints of tropical cyclone on three-dimensional structural characteristics of mesoscale oceanic eddies. Frontiers in Earth Science, 10: 1057798, doi: 10.3389/feart.2022.1057798

Zhou Hui, Nan Feng, Shi Maochong, et al. 2009. Characteristics of water exchange in the Luzon Strait during September 2006. Chinese Journal of Oceanology and Limnology, 27(30): 650–657

Zhou Hui, Yang Wenlong, Liu Hengchang, et al. 2017. The influence of typhoon *Haima* on warm eddies near the Luzon Strait and its dynamics. Oceanologia et Limnologia Sinica (in Chinese), 48(6): 1276–1288